Performance Analysis of Air-to-Water Optical Wireless Communication Using SPADs

Pooya Nabavi[1,2] and Murat Yuksel[1,2]
[1]Electrical and Computer Engineering, University of Central Florida, Orlando, FL USA 32816
[2]College of Optics and Photonics, University of Central Florida, Orlando, FL USA 32816
pooya.nabavi@knights.ucf.edu, murat.yuksel@ucf.edu

***Abstract*—Establishing highly reliable optical wireless communication links to submerged receivers exposed to insufficient light requires highly sensitive receivers with the ability to detect each photon carrying information. To this end, single photon avalanche diode (SPAD) receivers can be considered an appropriate option for the optical receiver system as they benefit from active quenching and biasing circuits, and offer a considerably high breaking voltage, providing the optical system with the ability to detect every single received photon in the ideal case. However, the sensitivity and bandwidth of the existing SPAD receivers have been limited by their dead time and limited photon detection efficiency. In this study, the performance of underwater SPAD receivers in detecting transmitted information from an optical transmitter located in the free space above the sea surface was assessed. To this end, the saddle-point approximation was used along with the Birnbaum-Saunders distribution to statistically model the fading coefficient of the air-to-water optical wireless communication channels and the statistical photon counting behavior of SPADs. The performance of the communication link was then assessed by obtaining the analytical relations for bit error rate. Finally, the results of numerical simulations are presented and the negative effects of dead time on information detection in the optical receiver system in various transmission bit rates are studied.**

***Index Terms*—Single Photon Avalanche Diode, Turbulence, Air-to-Water Optical Wireless Communications, Saddle-Point Approximation, Bit Error Rate.**

I. Introduction

The light was the first medium of communication since the dawn of civilization. For instance, a light beacon was used by Chinese soldiers in around 1,000 BC, and Romans used a polished surface to reflect sunlight to send messages to distant locations. Alexander G. Bell invented a wireless telephone system in 1880, also known as "photophone", which used reflected sunlight from a vibrating mirror as a transmission medium. With the advancement of technology and increased data volume, another wireless communication technology emerged which uses radio frequency (RF). RF communication has numerous advantages, such as reliability, non-line-of-sight (NLOS) operation, and omnidirectionality. Recently, optical wireless communication (OWC) is grabbing attention due to the spike in data demands, requirement of high bandwidth and data rate, and the need for secure communication. Even though OWC channels provide low-power and ultra-high data transmission rates than legacy RF channels, it suffers from various challenges such as absorption and scattering effect, the need for acquisition and maintenance of the line-of-sight (LOS), and moderate link ranges [1], [2].

In the last couple of decades, with ever-changing global climate, ocean exploration and research have become one of the most widely investigated research topics. Underwater wireless communication (UWC) opened up a tremendous opportunity for researchers to explore and acquire data from deep ocean remotely and safely. UWC technology can be realized by utilizing one of the three existing wireless carriers, i.e., acoustic waves, RF waves, and optical waves. Acoustic waves provide long communication range, but their low transmission rate, high latency, Doppler spread, and potential threat to marine life ultimately limit effective bandwidth and make it difficult to meet researchers' need. RF waves give quite a few benefits such as loose pointing requirements, moderately high data transmission rate, and tolerance to turbid water. However, RF wavelength is very lossy in seawater, hence it can provide link range up to 10 m only [3]. Optical waves, on the other hand, provide very high bandwidth, high transmission rate, low latency, and low power solution, but their communication range too is affected by other factors like scattering and dispersion [4].

In this paper, our goal is to study the efficacy of an optical receiver system for communication links from an aerial platform to a submerged vehicle. This type of OWC link technology is still emerging and under-explored. One of the major challenges for the air-to-water (A2W) OWC link is the air-water interface, which reflects and scatters signals and introduces a loss component that can over-power absorption loss. Even though RF waves have a relatively smooth transition at air-water boundaries, they experience very high absorption in sea-water, and hence, result in low communication range [1]. Thus, researchers have been exploring A2W-OWC possibilities as a solution. Darlis *et. al.* reported shore-to-undersea visible light communication, where the signal from a lighthouse is transmitted to an underwater platform through a buoy (relay) at the interface [5], but that defeats the purpose of security of the submerged platform. Chen *et. al.* experimentally demonstrated an A2W OWC system [6], however, they carried out the experiments with a controlled and static air-water interface under good pointing accuracy.

The detrimental impacts due to the above mentioned phenomena on the performance of the A2W OWC systems operating in photon starving environments has not yet been studied, which is the main focus of this work. Photodetectors used in the receiver is one of the most important components in optical communication systems, especially for establishing

a highly reliable link from the free space to the underwater environments. Most existing free-space optical systems use Avalanche Photodiodes (APD), as these photodiodes offer high bandwidth by maximizing the received signal-to-noise ratio, particularly in the free space. Furthermore, application of a reverse bias (i.e. cathode positive, anode negative) has greatly improved the speed of response and linearity of these devices. This is due to increase in the depletion region width and consequently decrease in junction capacitance. Applying a reverse bias, however, will increase the dark and noise currents. Moreover, given their low junction capacitance and, consequently, low rise and fall time, these detectors also provide a considerably high bandwidth for the receiver of the optical system, which in turn increases the reception bit rate. However, on the downside, the breaking voltage of these photodiodes is limited, preventing them to detect few single arrived photons in photon-starving environments such as seabeds with insufficient light. Moreover, although the avalanche multiplication process in these photodiodes intensifies the data-carrying signal, the process also increases the noise in the receiver of the optical system, further decreasing the sensitivity of these photodiodes in detection of the transmitted single photons.

II. Background: APDs vs. SPADs

The Single Photon Avalanche Diodes (SPAD) has been proposed recently in order to increase the sensitivity and ability of the system in detecting the single received photons. Avalanche photodiodes, which operate above the breakdown voltage in Geiger mode connected with avalanche-quenching circuits, can be used to detect single photons and are therefore called single photon avalanche diodes. The term SPAD defines a specifically designed category of APDs working with a reverse bias well above the breakdown voltage, in a way that completely differs from normal APDs, operated below the breakdown level [7].

Common silicon photodetectors are essentially pin diodes that are reverse biased: the incident light generates electron hole pairs in the depletion region contributing to the reverse current. The increase of the diode current is proportional to the incident light intensity. In order to have an internal gain between absorbed photons and output carriers, many APDs were proposed and developed. They operate just near, but below breakdown. Suitably designed active-quenching circuits (AQC) make it possible to exploit the best performance of SPADs. Thick silicon SPADs that operate at high voltages (250-450 V) have photon detection efficiency higher than $\%50$ from 540 nm to 850 nm wavelength and still $\%3$ at 1064 nm. Thin silicon SPADs that operate at low voltages (10-50 V) have $\%45$ efficiency at 500 nm, declining to $\%10$ at 830 nm and to as little as $\%0.1$ at 1064 nm [8]. The achieved minimum counting dead time and maximum counting rate are 40 ns and 10 Mcps with thick silicon SPADs, and 10 ns and 40 Mcps with thin SPADs [8], [9].

In the literature, SPADs have also been referred to as Geiger-mode avalanche photodiodes or triggered avalanche detectors [9], [10]. Unlike APDs, SPADs act as photo detectors when operated at a voltage higher than their breakdown threshold voltage. A single photon causes an avalanche of electrons producing a large current pulse for a single photon. SPADs are more suitable for photon-starving conditions where Charged Coupled Devices (CCDs) and regular APDs are inherently unable to provide accurate measurements of high speed low intensity of light at high frame rates. Thin-junction SPADs have breakdown voltage of 10 to 50 V, small active area, with diameter from $20\mu m$ to 100 μm, and fairly good quantum efficiency in the visible range, about $\%45$ at 500 nm. The circuit that quenches the avalanche and resets the bias voltage plays a key role in the SPAD detector performance. But even by using the AQCs the dead time is neither well known, nor very stable. The result is a loss of linearity at high counting rates, which may be measured empirically.

Compared to APDs, these detectors offer a considerably higher responsivity and sensitivity, as well as a considerably higher breaking voltage, which itself positively affects the sensitivity level [11]. The disadvantages of the SPAD photo detection include their smaller active detection area, the quenching process required for appropriately biasing these detectors which itself causes them to become blind and unresponsive for slight time duration (also referred to as dead time) after detection of single received photons. This duration in which the SPAD detectors lose their ability to detect and count the received photons is called dead time, the value of which ranges from a maximum of 35 ns and minimum of 5 ns per photon count. Dead time introduced significantly decreases our performance and limits our overall available bandwidth for high speed data communications.

Major contributions of our work include:

- Modeling of performance of A2W-OWC links using SPADs by utilizing water-air interface model based on Birnbaum-Saunders distribution for fading coefficient of the channel,
- Evaluation of the effect of sea-surface waves on the A2W-OWC links,
- Utilizing photon counting methods such as Saddle-Point approximation to obtain an analytical expression for the BER of W2A-OWC links,
- Evaluating the detrimental effects of the detector's dead time and turbulence-induced channel delay spread,
- Quantitative expression of the relationship between the sea-surface waves' strength and the optimum tuning of the SPADs in terms of dead time.

III. System Model

On transmitter side, we assume On-Off Keying (OOK) modulation, i.e., 1s represented with high light intensity and 0s with low. As a result, the transmitted data sequence can be expressed as:

$$x(t) = \sum_{m=0}^{\infty} b_m P(t - mT_b) \tag{1}$$

where $b_m \in [0, 1]$ is the OOK-modulated signal corresponding to the m^{th} transmitted bit (or symbol), and $T_b = \frac{1}{R_b}$ is the bit

duration time for data transmission rate of R_b (b/s). Moreover, in this scheme, bits "0" and "1" of each time slot will be transmitted with pulse shapes 0 and $P(t)$, respectively.

On the receiver side installed on the submerged vehicle, the SPAD generates a data-carrying photo current which will be converted to a voltage signal by a wide bandwidth transimpedance and will be further amplified. When a photon hits a conventional APD, the generated output photo-current of the APD (i.e., the total number of generated photo-electrons) obeys a Poisson distribution [12], and the output of the integrator can be modeled as a Poisson Point Process whose average is in proportion with the total optical incident power [12], [13]. However, SPAD detectors, thanks to their higher breaking voltage, offer a considerably higher sensitivity compared to the conventional APDs. However, the quenching process required for appropriately biasing these detectors causes them to become unresponsive for time duration after each photon detection. This duration in which the SPAD detectors lose their ability to detect and count the received photons is called *dead time* τ, the value of which ranges from 5 ns to 35 ns per photon count. When the SPAD dead time is considered, the photon counts are no longer Poisson distributed. Assuming that the SPAD detector is ready to operate at the beginning of the counting interval, the maximum observable photon count during this period is $n_{max} = \lceil \frac{T_b}{\tau} \rceil$.

A. Photon Count for Constant Fading

When a photon hits an SPAD, the generated output photo-current (i.e., the total number of generated photo-electrons) can be expressed in terms of Poisson distributions. In particular, the probability of n photons being detected during the time interval of [0, T_b] given the channel's fading coefficient $\tilde{H}$ is equal to a constant number $\tilde{h}$ obeys the following distribution [14]–[16]:

$$\Pr\left\{N\left(T_b\right)=n|\tilde{H}=\tilde{h}\right\}= \tag{2}$$
$$\begin{cases} \theta\left(0,\,\lambda_0\right) & ;\, n=0 \\ \sum\limits_{i=0}^{n}\theta\left(i,\,\lambda_n\right)-\sum\limits_{i=0}^{n-1}\theta\left(i,\,\lambda_{n-1}\right) & ;\, 1\le n<n_{max} \\ 1-\sum\limits_{i=0}^{n-1}\theta\left(i,\,\lambda_{n-1}\right) & ;\, n=n_{max} \\ 0 & ;\, n>n_{max} \end{cases}$$

where λ_n is the average number of detected photoelectrons when n photons arrive at the SPAD during the observation time of T_b. $\theta(i,X) \triangleq \frac{X^i e^{-X}}{i!}$ is the Poisson function that computes the probability of receiving i photons when X is the average photon count arriving at the SPAD during the observation time of T_b. Given dead time of τ and the channel's fading coefficient $\tilde{H}=\tilde{h}$, λ_n can be obtained as:

$$\begin{aligned}\lambda_n &= \int_0^{(T_b-n\tau)} \frac{\left(\mathcal{R}_\lambda \times \frac{hf}{q}\right)\times\Gamma\left(t\right)}{hf}\mathrm{d}t \\ &= \frac{\mathcal{R}_\lambda}{q}\times P_i \times \tilde{h}\times(T_b-n\tau) \quad i=0,1\end{aligned} \tag{3}$$

where $\mathcal{R}_\lambda = \frac{\eta_Q q}{hf}$ is the responsivity of the SPAD at the corresponding wavelength λ of the incident light, which we assume to be Green color, i.e., $\lambda = 532$ nm. η_Q represents the quantum efficiency (i.e., the number of emitted electrons per number of incident photons). $P_0 = 0$ and $P_1 = \int_0^{T_b} P(t)\mathrm{d}t$ are average power levels of the emitted radiation when bits "0" and "1" are sent, respectively. $q = 1.602\times10^{-19}C$ is the elementary charge, $h = 6.626\times10^{-34}$ is Plank's constant, and f represents the frequency of the light source [17]. Further, $\Gamma(t) = h(t) * P(t)$ where $h(t) = \tilde{H}\delta(t)$ is the impulse response of the A2W channel, $\delta(t)$ is the Dirac function and $\tilde{H}$ is a positive multiplicative fading coefficient.

B. Fading Distribution for A2W OWC Channel

In our earlier study [18], we empirically characterized the dominant turbulence effects of aquatic random waves on the channel's water to air interface, and estimated the resulting fading to be following a Birnbaum-Saunders distribution as follows:

$$\begin{aligned}f_{\tilde{H}}(\tilde{h}) =& \frac{1}{\sqrt{2\pi}}\exp\left[-\frac{\left(\sqrt{\frac{\tilde{h}-\mu}{\beta}}-\sqrt{\frac{\beta}{\tilde{h}-\mu}}\right)^2}{2\gamma^2}\right]\times \\ & \left[\frac{\left(\sqrt{\frac{\tilde{h}-\mu}{\beta}}+\sqrt{\frac{\beta}{\tilde{h}-\mu}}\right)^2}{2\gamma\tilde{h}}\right];\ \tilde{h}>0\end{aligned} \tag{4}$$

where $\gamma > 0$ is the shape parameter, μ is the location parameter, and $\beta > 0$ is the scale parameter – all of which were empirically measured in [18].

C. Photon Count Distribution for Varying Fading

To obtain unconditional photon count distribution, we use Eq. (2) and Eq. (4). We obtain the probability of receiving n photons during T_b time interval as

$$\Pr\left\{N(T_b)=n\right\} = \int_0^\infty \Pr\left\{N\left(T_b\right)=n|\tilde{H}=\tilde{h}\right\} f_{\tilde{H}}(\tilde{h})\,\mathrm{d}\tilde{h}. \tag{5}$$

Further, we write the mean and the variance of the photon count distribution, respectively, as:

$$\mu_N = \int_0^\infty \left[n_{max} - \sum_{j=0}^{(n_{max}-1)}\sum_{i=0}^{j}\theta\left(i,\,\lambda_j\right)\right] f_{\tilde{H}}(\tilde{h})\mathrm{d}\tilde{h} \tag{6}$$

and

$$\begin{aligned}\sigma_N^2 = \int_0^\infty \Bigg[& \sum_{j=0}^{(n_{max}-1)}\sum_{i=0}^{j}\left(2n_{max}-2j-1\right)\theta\left(i,\lambda_j\right) - \\ & \left(\sum_{j=0}^{(n_{max}-1)}\sum_{i=0}^{j}\theta\left(i,\lambda_j\right)\right)^2\Bigg] f_{\tilde{H}}(\tilde{h})\ \mathrm{d}\tilde{h}.\end{aligned} \tag{7}$$

Thus far, we have modeled the photon count detected by an SPAD in a A2W OWC channel. Next, we will calculate the photocurrent generated by the SPAD output, which we will use for deciding if a "0" or "1" was sent.

D. Photocurrent Generated from SPAD

The output current of the SPAD can be modeled as:

$$\begin{aligned} U = I_o(T_b) &= \frac{N_R \times q}{\Delta t} + I_T \\ &= \frac{\mu_{N_R} \times q}{\Delta t} + \frac{(N_R - \mu_{N_R}) \times q}{\Delta t} + I_T \\ &= I_{avg} + I_s + I_T \end{aligned} \tag{8}$$

where $\Delta t = \frac{1}{2B}$ is the Nyquist sampling time assuming B is the receiver's bandwidth. $N_R = N + N_{BG} + N_D$ is the total number of received photoelectrons due to arrival of data-carrying photoelectrons N, noise photoelectrons due to background light N_{BG}, and SPAD's dark current N_D during the detection of a symbol in the receiver. N is the count of photoelectrons generated from the received data-carrying signal, and its distribution, first and second moments can be obtained according to Eq. (5), Eq. (6) and Eq. (7) respectively. Furthermore, μ_{N_R} is the mean value of N_R and is equal to sum of the average values of N, N_{BG} and N_D. Since dark current and background light are both Poisson [19], [20], we can write $\mu_{N_R} = \mu_N + \sigma^2_{BG} + \sigma^2_D$ as the latter two's mean and variance are expected to be the same.

The dark and the background light's photo-count variances (or equivalently their averages) can be written as $\sigma^2_D = \frac{2I_{dc}BT_b}{q}$ and $\sigma^2_{BG} = \frac{2\eta_Q P_{BG} T_b}{hf}$, respectively. Here, P_{BG} is the received background power and I_{dc} is the dark current of SPAD hardware. I_T is a thermal noise current and it is assumed to be Gaussian distributed with variance $\sigma^2_T = \frac{4K_B T_e B F_n}{R_L}$ and mean value $\mu_T = 0$. K_B, T_e, R_L and F_n are Boltzmann's constant, the receiver equivalent temperature, load resistance and receiver's noise figure, respectively. $I_s \triangleq \frac{(N_R - \mu_{N_R}) \times q}{\Delta t}$ is the shot noise with mean value $\mu_s = 0$ and variance of $\sigma^2_s = 4q^2B^2(\sigma^2_N + \sigma^2_D + \sigma^2_{BG})$. $I_{avg} \triangleq \frac{\mu_{N_R} \times q}{\Delta t}$ is the deterministic average output current.

IV. Link Performance Analysis Using Saddle-point Photon-Counting Method

In this section, given the output current from an SPAD underwater Eq. (8), we derive the required expressions for the system Bit Error Ratio (BER) using a photon-counting approach. We consider signal-dependent shot noise, dark current, and background light all to be Poisson. Further, we model the thermal noise with a Gaussian distribution. Based on Saddle-Point Approximation [12], [19], the system BER can be obtained as $BER = \frac{1}{2}\left[q_+(I_{th}) + q_-(I_{th})\right]$, where $q_+(I_{th})$ and $q_-(I_{th})$ are probabilities of error when bits 0 and 1 are sent. We can write $q_+(I_{th})$ and $q_-(I_{th})$ as

$$\begin{aligned} q_+(I_{th}) &\triangleq \Pr(U > I_{th} | zero) \approx \frac{\exp\left[\Psi_0(s_0)\right]}{\sqrt{2\pi\Psi_0''(s_0)}} \\ q_-(I_{th}) &\triangleq \Pr(U \leq I_{th} | one) \approx \frac{\exp\left[\Psi_1(s_1)\right]}{\sqrt{2\pi\Psi_1''(s_1)}} \\ \Psi_0(s) &\triangleq \ln\left[\phi_{U,0}(s)\right] - sI_{th} - \ln|s| \\ \Psi_1(s) &\triangleq \ln\left[\phi_{U,1}(s)\right] - sI_{th} - \ln|s| \end{aligned} \tag{9}$$

where U is the received photocurrent during interval of $[0, T_b]$ and is obtained according to Eq. (8). Furthermore, s_0 is the positive and real root of $\Psi_0'(s)$, i.e., $\frac{\mathrm{d}\Psi_0(s)}{\mathrm{d}s}|_{s=s_0} = 0$ and s_1 is the negative and real root of $\Psi_1'(s)$, i.e., $\frac{\mathrm{d}\Psi_1(s)}{\mathrm{d}s}|_{s=s_1} = 0$. I_{th} is the optimum current threshold used in the receiver for optimum detection and can be optimally calculated to minimize the BER, i.e., $\frac{\mathrm{d}BER}{\mathrm{d}I_{th}} = 0$. $\phi_{U,0}(s)$ and $\phi_{U,1}(s)$ are moment generating functions (MGF) of the receiver's output photocurrent (U) when bits "0" and "1" are transmitted, respectively and can be obtained according Eqs. (10)-(13)

$$\phi_U(s) = \int_0^\infty \phi_{U|\tilde{H}=\tilde{h}}(s) f_{\tilde{H}}(\tilde{h}) \mathrm{d}\tilde{h} \tag{10}$$

$$\begin{aligned} \phi_{U|\tilde{H}=\tilde{h}}(s) &= E\left\{e^{sU} | \tilde{H} = \tilde{h}\right\} = \\ &= E\left\{e^{s\frac{qN}{\Delta t}} | \tilde{H} = \tilde{h}\right\} \times E\left\{e^{s\frac{q(N_{BG}+N_D)}{\Delta t}}\right\} \times E\left\{e^{sI_T}\right\} \\ &= \left[\sum_{n=0}^{n_{max}} \left[e^{2qBsn} \Pr\left\{N(T_b) = n | \tilde{H} = \tilde{h}\right\}\right]\right] \times \\ &\exp\left[(\sigma^2_{BG} + \sigma^2_D)\left(\exp(2qBs) - 1\right) + \exp(\frac{s^2\sigma^2_T}{2})\right] \end{aligned} \tag{11}$$

$$\phi_{U,0}(s) \triangleq \phi_U(s)|_{\text{Bit 0 is sent i.e., } (\lambda_n|_{i=0})} \tag{12}$$

$$\phi_{U,1}(s) \triangleq \phi_U(s)|_{\text{Bit 1 is sent i.e., } (\lambda_n|_{i=1})} \tag{13}$$

and as a result the BER can be numerically computed as

$$\begin{aligned} BER &= \frac{1}{2}(q_+(I_{th}) + q_-(I_{th})) = \\ &= \frac{1}{2}\left[\frac{\exp\left[\Psi_0(s_0)\right]}{\sqrt{2\pi\Psi_0''(s_0)}} + \frac{\exp\left[\Psi_1(s_1)\right]}{\sqrt{2\pi\Psi_1''(s_1)}}\right] \end{aligned} \tag{14}$$

Appendix A details how the expression in Eq.(14) is calculated. However, to calculate the BER above, the roots for s_0, s_1, I_{th} are necessary. To obtain these roots, we utilize the Quasi-Newton Method by solving the following system of nonlinear equations for s_0, s_1, $I_{th} \in \mathbb{R}$:

1) $\frac{\mathrm{d}\Psi_0(s)}{\mathrm{d}s}|_{s=s_0} = 0$
2) $\frac{\mathrm{d}\Psi_1(s)}{\mathrm{d}s}|_{s=s_1} = 0$
3) $\frac{\mathrm{d}BER}{\mathrm{d}I_{th}} = 0.$

We, then, use the solutions for s_0, s_1 and I_{th} for calculating the most accurate approximation of BER.

V. Results and Discussion

In this section, we provide the numerical results for the BER performance of SPAD receivers operating underwater in A2W channels in various configurations, including the SPAD's dead time and fading characteristics of A2W channels containing random surface waves. For BER analysis of the link we use the saddle-point approximation considering the exact photon counting statistics of SPADs. The parameters used for simulating the operation of the A2W communication link including an SPAD receiver are listed in Table 1.

BER increases with dead time and bit rate. Fig. 1(a) shows the performance of SPAD receivers with different dead times in detection of received symbols at different transmission bit rates when A2W interface contains random aquatic waves. We observe that SPAD receivers are a viable option for high

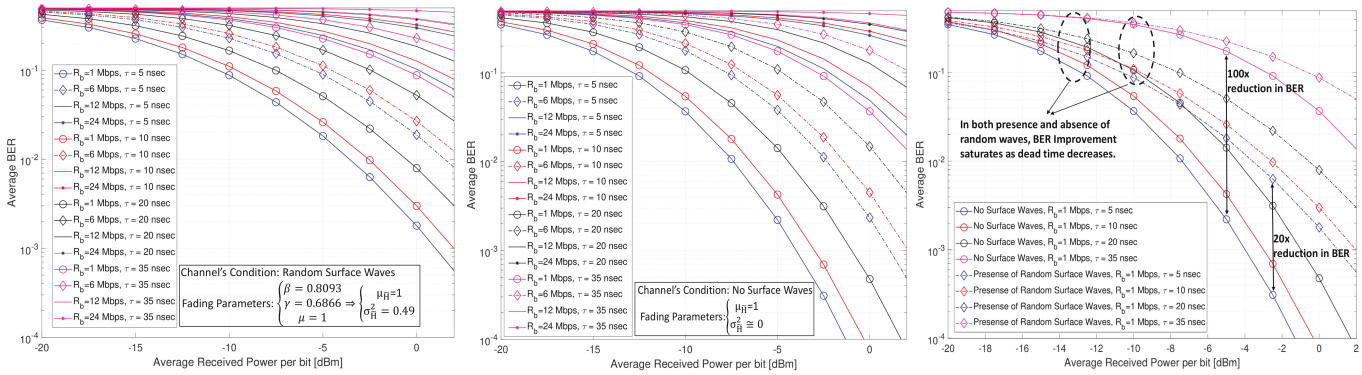

Fig. 1. BER performance of SPAD receivers with various dead times, operating in A2W channels: (a) Random surface waves; (b) No surface waves; (c) BER performance at transmission rate of R_b= 1 Mbps, with or without random surface waves.

speed A2W OWC, e.g., BER is $\approx 10^{-2}$ for -5 dBm receive power even at very conservative dead times such as 5 ns. As shown, at all bit rates, as the dead time of the optical system increases and approaches the bit time, the system performance in detecting the transmitted bits decreases. This necessitates the need for designing and implementing high-efficiency quenching biasing circuits to achieve higher reception bit rates and reduce BER. Moreover, as shown in the figure, for a given dead time, increasing the bit rate increases BER, which is due to the inter-symbol interference (ISI) in A2W channels containing random aquatic waves at the interface. In other words, as the bit rate increases, the bit time first approaches the delay spread existing in the A2W channel, and then the dead time caused by the SPAD receivers. This increases the uncertainty when detecting the symbols received in the receiver of the optical system (even at a small dead time of 5 ns), consequently increasing the BER.

Effect of bit rate on BER increases if no surface waves exist. Fig. 1(b) evaluates the performance of the receiver with different dead times in detection of received symbols at different transmission bit rates in the absence of aquatic waves at the interface of the free space and underwater channels. As expected, increasing the dead time of the receiver in the optical system reduces its performance in detection of transmitted bits. Moreover, as the bit time approaches the dead time of the SPAD receiver, the decision-making uncertainty is increased in detection of the received symbols.

Dead time affects BER more adversely than surface waves. Fig. 1(c) compares the performance of SPAD receivers with different dead times, at transmission rate of 1 Mbps, in both presence and absence of random surface waves at the A2W interface. As shown, random surface waves at the A2W interface leads to a loss of performance in detecting received signals at all dead times. This can be attributed to substantially higher delay spreads in the A2W channel in presence of random surface waves. Further, we observe that halving the dead time of SPAD reduces the BER by ≈100 times. This implies that SPAD's dead time is the crucial parameter for the A2W OWC links.

TABLE I
SYSTEM PARAMETERS USED IN SIMULATIONS.

Coefficient	Value
Quantum efficiency, η_Q	0.7
Wavelength, λ	532 nm
Dark current [19], I_{dc}	1.226×10^{-9} A
Equivalent temperature, T_e	290 K
Load resistance, R_L	100 Ω
Electronic bandwidth, B	200 MHz
Background Power [12], P_{BG}	7.68×10^{-9} W
Noise Figure, F_n	2
Fading (Random Waves) [18], $\{\beta,\gamma,\mu\}$	$\{0.8093, 0.6866, 1\}$

VI. CONCLUSION

In this paper, an analytical BER expression for the impact of dead time and random surface waves at the cross-section of A2W channels has been derived and utilized to evaluate the system's performance in various transmission bit rates. Moreover, this study evaluated the performance of SPAD receivers located underwater in detection of transmitted data from an optical transmitter fixed in the free-space. To this end, by leveraging the statistical photon counting behavior of SPADs, the analytical relations for BER were derived using the saddle-point approximation method along with the Birnbaum-Saunders fading statistical model. Based on the numerical simulation results, the negative effects of dead time caused by the SPAD receivers and the ISI caused by the aquatic wave turbulence at the A2W interface were studied.

We observed that, for a given dead time, increasing the bit rate increases the probability of bit error, which is due to the ISI in the channel containing random waves at the A2W interface. By increasing the bit rate, the bit time approaches the dead time of SPAD receivers, and then the delay spread in the A2W channel. This, in turn, increases the uncertainty when detecting the received symbols in the receiver of the optical system (even at a small dead time of 5 ns), consequently decreasing the performance of the system and increasing the BER. Our results show that SPAD receivers can be used in realizing high speed A2W OWC links. Further, they imply that designing efficient quenching circuits for SPAD receiver is the key enabler for their practical use.

APPENDIX A
SADDLE-POINT APPROXIMATION OF BER

Following Helstrom [19], G. Einerson has derived a numerically simple approximation to the cumulative probability

distribution of a continuous stochastic variable with density $p(x)$ [12]. Let $q_+(\alpha)$ denote the upper tail

$$q_+(\alpha) = \int_{\alpha}^{\infty} p(x)dx \tag{15}$$

and

$$q_-(\alpha) = \int_{-\infty}^{\alpha} p(x)dx \tag{16}$$

the lower tail of the probability distribution. The bilateral Laplace transform of $p(x)$ can be expressed in term of the moment generating function as

$$\Psi(-s) = \int_{-\infty}^{\infty} e^{-sx}dx \tag{17}$$

The probability density $p(x)$ is equal to the inverse integral

$$p(x) = \frac{1}{2\pi j}\int_{c-j\infty}^{c+j\infty} \Psi(-s)e^{sx}ds \tag{18}$$

where c is in the convergence region of the transform.

By replacing $p(x)$ in (15) with (18) and choosing the contour of integration such that $c < 0$ to guarantee convergence of the integral, the resulting lower tail is

$$q_+(\alpha) = \frac{1}{2\pi j}\int_{c-j\infty}^{c+j\infty} \frac{e^{s\alpha}}{s}\Psi(-s)ds.$$

Changing the integration variable from $-s$ to s gives

$$q_+(\alpha) = \frac{1}{2\pi j}\int_{c-j\infty}^{c+j\infty} \frac{e^{-s\alpha}}{s}\Psi(-s)ds; \quad c > 0. \tag{19}$$

The parameter c is chosen to be s for which the integrand is minimal. It turns out $s = s_0$ corresponds to a saddle-point in complex plane, hence the name of the method. The integrand in terms of a 'phase' function $\psi(s)$ is defined by

$$\exp[\psi(s)] = |s|^{-1}\exp(-s\alpha)\Psi(s) \tag{20}$$

The function $\psi(s)$ is expanded in a Taylor series around the point $s = s_0$:

$$\psi(s) = \psi(s_0) + \frac{1}{2}\psi^{''}(s_0)(s - s_0)^2 + \dots \tag{21}$$

The first derivative does not appear since $s = s_0$ is an extremum of $\psi(s)$.

Substitution of (21) into (19) and neglecting higher-order terms yields the saddle-point approximation:

$$\begin{aligned} q_-(\alpha) &\approx \frac{1}{2\pi}\exp[\psi(s_0)]\int_{-\infty}^{\infty}\exp\left[-\frac{1}{2}\psi^{''}(s_0)y^2\right]dy \\ &= \left[2\pi\psi^{''}(s_0)\right]^{-1/2}\exp[\psi(s_0)] \end{aligned} \tag{22}$$

The parameter s_0 is the value of s for which $\psi(s)$ has a minimum. It is equal to the positive root of the equation:

$$\psi^{'}(s) = 0 \tag{23}$$

For the lower tail, analogously to (19),

$$q_-(\alpha) = \frac{-1}{2\pi j}\int_{c-j\infty}^{c+j\infty} \frac{e^{-s\alpha}}{s}\Psi(s)ds \tag{24}$$

with $c < 0$. Expansion of $\psi(s)$ in a Taylor series and integration gives:

$$q_-(\alpha) \approx [2\pi\psi^{''}(s_1)]^{-1/2}\exp[\psi(s_1)] \tag{25}$$

with s_1 equal to the negative root of (23).

REFERENCES

[1] Z. Zeng, S. Fu, H. Zhang, Y. Dong, and J. Cheng, "A survey of underwater optical wireless communications," *IEEE communications surveys & tutorials*, vol. 19, no. 1, pp. 204–238, 2017.

[2] S. S. Polkoo and C. K. Renshaw, "Imaging-based beam steering for free-space optical communication," *Appl. Opt.*, vol. 58, no. 13, pp. D12–D21, May 2019. [Online]. Available: http://ao.osa.org/abstract.cfm?URI=ao-58-13-D12

[3] H. Kaushal and G. Kaddoum, "Underwater optical wireless communication," *IEEE access*, vol. 4, pp. 1518–1547, 2016.

[4] X. Yi, Z. Li, and Z. Liu, "Underwater optical communication performance for laser beam propagation through weak oceanic turbulence," *Applied Optics*, vol. 54, no. 6, pp. 1273–1278, 2015.

[5] A. R. Darlis, W. A. Cahyadi, and Y.-H. Chung, "Shore-to-undersea visible light communication," *Wireless Personal Communications*, vol. 99, no. 2, pp. 681–694, 2018.

[6] Y. Chen, M. Kong, T. Ali, J. Wang, R. Sarwar, J. Han, C. Guo, B. Sun, N. Deng, and J. Xu, "26 m/5.5 Gbps air-water optical wireless communication based on an OFDM-modulated 520-nm laser diode," *Optics express*, vol. 25, no. 13, pp. 14 760–14 765, 2017.

[7] L. Zhang, D. Chitnis, H. Chun, S. Rajbhandari, G. Faulkner, D. O'Brien, and S. Collins, "A comparison of apd-and spad-based receivers for visible light communications," *Journal of Lightwave Technology*, vol. 36, no. 12, pp. 2435–2442, 2018.

[8] S. Cova, M. Ghioni, A. Lacaita, C. Samori, and F. Zappa, "Avalanche photodiodes and quenching circuits for single-photon detection," *Appl. Opt.*, vol. 35, no. 12, pp. 1956–1976, Apr 1996.

[9] F. Zappa, S. Tisa, A. Tosi, and S. Cova, "Principles and features of single-photon avalanche diode arrays," *Sensors and Actuators A: Physical*, vol. 140, no. 1, pp. 103–112, 2007.

[10] D. Renker, "Geiger-mode avalanche photodiodes, history, properties and problems," *Nuclear Instruments and Methods in Physics Research Section A: Accelerators, Spectrometers, Detectors and Associated Equipment*, vol. 567, no. 1, pp. 48–56, 2006.

[11] L. Zhang, H. Chun, G. Faulkner, D. O'Brien, and S. Collins, "A comparison between the sensitivities of vlc receivers containing an off-the-shelf spad array and an apd," in *2017 IEEE Photonics Conference (IPC)*, Oct 2017, pp. 27–28.

[12] R. M. Gagliardi and S. Karp, *Optical Communications*. New York: Wiley, 1995.

[13] M. V. Jamali, A. Mirani, A. Parsay, B. Abolhassani, P. Nabavi, A. Chizari, P. Khorramshahi, S. Abdollahramezani, and J. A. Salehi, "Statistical studies of fading in underwater wireless optical channels in the presence of air bubble, temperature, and salinity random variations," *IEEE Transactions on Communications*, vol. 66, no. 10, pp. 4706–4723, Oct 2018.

[14] E. Sarbazi and H. Haas, "Detection statistics and error performance of spad-based optical receivers," in *2015 IEEE 26th Annual International Symposium on Personal, Indoor, and Mobile Radio Communications (PIMRC)*. IEEE, 2015, pp. 830–834.

[15] M. Teich and B. Cantor, "Information, error, and imaging in deadtime-perturbed doubly stochastic poisson counting systems," *IEEE Journal of Quantum Electronics*, vol. 14, no. 12, pp. 993–1003, 1978.

[16] C. Wang, H.-Y. Yu, Y.-J. Zhu, T. Wang, and Y.-W. Ji, "Experimental study on spad-based vlc systems with an led status indicator," *Optics Express*, vol. 25, no. 23, pp. 28 783–28 793, 2017.

[17] M. V. Jamali, P. Nabavi, and J. A. Salehi, "Mimo underwater visible light communications: Comprehensive channel study, performance analysis, and multiple-symbol detection," *IEEE Transactions on Vehicular Technology*, vol. 67, no. 9, pp. 8223–8237, 2018.

[18] P. Nabavi, A. F. M. S. Haq, and M. Yuksel, "Empirical modeling and analysis of water-to-air optical wireless communication channels," in *2019 IEEE International Conference on Communications Workshops (ICC Workshops)*, May 2019, pp. 1–6.

[19] G. Einarsson, *Principles of Lightwave Communications*. New York: Wiley, 1996.

[20] P. Nabavi and M. Yuksel, "Conformal vlc receivers with photodetector arrays: Design, analysis and prototype," in *ICC 2019 - 2019 IEEE International Conference on Communications (ICC)*, May 2019, pp. 1–7.